

# Journal of Astronomical Telescopes, Instruments, and Systems

AstronomicalTelescopes.SPIEDigitalLibrary.org

## **Optical design of the Extreme Coronagraph for Living Planetary Systems instrument for the LUVOIR mission study**

Qian Gong  
Matthew R. Bolcar  
James A. Corsetti  
Julie A. Crooke  
Joseph Generie  
Tyler D. Groff  
Jason Hylan  
Andrew Jones  
Roser Juanola Parramon  
Avi M. Mandell  
Garrett J. West  
Neil T. Zimmerman

Qian Gong, Matthew R. Bolcar, James A. Corsetti, Julie A. Crooke, Joseph Generie, Tyler D. Groff, Jason Hylan, Andrew Jones, Roser Juanola Parramon, Avi M. Mandell, Garrett J. West, Neil T. Zimmerman, "Optical design of the Extreme Coronagraph for Living Planetary Systems instrument for the LUVOIR mission study," *J. Astron. Telesc. Instrum. Syst.* **5**(2), 025002 (2019), doi: 10.1117/1.JATIS.5.2.025002.

**SPIE.**

# Optical design of the Extreme Coronagraph for Living Planetary Systems instrument for the LUVOIR mission study

Qian Gong,\* Matthew R. Bolcar, James A. Corsetti, Julie A. Crooke, Joseph Generie, Tyler D. Groff, Jason Hylan, Andrew Jones, Roser Juanola Parramon, Avi M. Mandell, Garrett J. West, and Neil T. Zimmerman  
NASA Goddard Space Flight Center, Greenbelt, Maryland, United States

**Abstract.** The large UV/optical/IR surveyor (LUVOIR) is a concept for a highly capable, multiwavelength space observatory with ambitious science goals. Finding and characterizing a wide range of exoplanets, including those that might be habitable, is a major goal of the study. The ambitious science goals drive the challenges of optical design. This paper will present how the optical design meets the unique challenges for coronagraphs on large telescopes to achieve high contrast for a wide wavelength range from 200 to 2000 nm. Some of these unique challenges include the position and size of occulter masks, deformable mirror placement and separation, tight tolerances on the optical system and each element, and finally, packaging all instruments in a limited space. Three types of modules are designed after the coronagraph to explore the exoplanets and analyze the spectrum of detected exoplanet signals: two imaging cameras, two integral field spectrographs, and one high-resolution spectrometer. All of them work together to provide information to meet scientific challenges in searching for habitable planets. The optical designs, unique challenges, and the solutions for all coronagraph and spectral modules are presented. Their specifications derived from science goals are also presented. © The Authors. Published by SPIE under a Creative Commons Attribution 4.0 Unported License. Distribution or reproduction of this work in whole or in part requires full attribution of the original publication, including its DOI. [DOI: [10.1117/1.JATIS.5.2.025002](https://doi.org/10.1117/1.JATIS.5.2.025002)]

Keywords: exoplanets; coronagraph; integral field spectrograph; high-resolution spectrometer.

Paper 18089 received Oct. 22, 2018; accepted for publication Apr. 12, 2019; published online May 9, 2019.

## 1 Introduction

The main goals of large UV/optical/IR surveyor (LUVOIR) are to investigate astrophysics, exoplanets, the cosmic origins, and the Solar System.<sup>1</sup> The exoplanets investigation will be accomplished by the Extreme Coronagraph for Living Planetary Systems (ECLIPS) instrument: an ultrahigh contrast coronagraph with imaging cameras and integral field spectrographs (IFS) spanning 200 to 2000 nm, capable of directly observing a wide range of exoplanets and obtaining spectra of their atmospheres.

The first confirmed exoplanet detection occurred in 1992.<sup>2</sup> Since then, there have been several thousand more confirmed detections. The ECLIPS instrument in the LUVOIR mission is aimed to elevate the study to a stage: exploring the full diversity of exoplanets; discovering and characterizing exoplanets in the habitable zones of Sun-like stars across a range of ages; and searching for biosignatures in their atmospheres, in a survey large enough to provide evidence for (or against) the presence of habitable planets and life.<sup>3</sup>

To achieve these ambitious goals, a large telescope is necessary. The three major advantages of a large telescope for coronagraphy are the following:

1. High photon collection power to increase exoplanet detection yields,<sup>4</sup> providing the ability to detect exoplanets in the habitable zones with higher signal-to-noise ratio (SNR).

2. A larger aperture enables a smaller inner working angle (IWA) or minimum observable separation between an exoplanet and the host star. The IWA is characterized by the parameter  $\lambda/D$ , where  $\lambda$  is the observing wavelength and  $D$  is the telescope aperture diameter. It is noted that the plate scale of a coronagraph increases linearly with the entrance pupil diameter for a fixed  $f/\#$ . As a result, for any selected exoplanet with a given angular separation in the sky, then the required IWA for a large telescope can be relaxed. For example, for an exoplanet that is 50 mas from its host star, the required IWA for a 4-m telescope observing at 500 nm is  $\sim 1.9 \lambda/D$ . For a 15-m telescope, the IWA is  $\sim 7.3 \lambda/D$ . This higher resolution provides an advantage in detecting exoplanets in the habitable zones for more distant stars.
3. In order to determine if an exoplanet in the habitable zone is indeed habitable, its spectrum has to be analyzed. The photons collected from large telescopes like LUVOIR provide enough SNR for desired spectrometers, such as the IFS and high-resolution spectrometer (HRS).

Combining the science needs and engineering feasibility, ECLIPS is designed to have three coronagraph channels: the ultraviolet (UV) channel has one direct imaging camera, the optical channel has both a direct imager and an IFS, and the near-infrared (NIR) channel has an IFS and HRS. Two telescope architectures are currently being investigated under the LUVOIR study: a 15-m obscured aperture telescope and an

\*Address all correspondence to Qian Gong, E-mail: [qian.gong-1@nasa.gov](mailto:qian.gong-1@nasa.gov)

**Table 1** ECLIPS top level requirement from science goals.

Ultrahigh contrast coronagraph	$10^{-10}$
Total bandwidth	200–2000 nm
IWA	$\sim 3.5 \lambda/D$
Outer working angle	$\sim 64 \lambda/D$
Imaging and imaging spectroscopy	VIS IFS $R = 140$ , NIR IFS $R = 70$ , NIR HRS $R = 200$

8-m unobscured aperture telescope (named LUVOIR-A and LUVOIR-B, respectively).

The top requirements derived from the exoplanet exploration goals for LUVOIR are listed in Table 1. More details on the flow down of the science goals to the engineering requirements can be found in the LUVOIR Study interim report.<sup>3</sup> To derive optical design specifications from top-level requirement, the following engineering factors must be considered:

1. The coronagraph must be able to accommodate the needed elements, such as coronagraph masks, deformable mirrors (DMs), spectral filters, etc., to achieve the required contrast of  $10^{-10}$ .
2. To reach the full wavelength range, ECLIPS must be divided into separate channels that are compatible with detector technologies for the UV, optical, and NIR.
3. The optical system throughput directly affects the exoplanet detection yield. Wherever possible the number of optical elements must be minimized. Optical coatings and material transmittances must also be carefully selected.
4. The wavelength that divides each channel is chosen to be in the continuum, avoiding key spectral features critical to science.
5. The imaging spectrometers must provide the spectral resolving power required to detect spectral features associated with key biosignatures.

Based on the considerations above, the ECLIPS instrument is divided into three channels: UV, VIS, and NIR. The three channels operate simultaneously to observe the entire ECLIPS wavelength range of 200 nm to 2.0  $\mu\text{m}$ . Nonabsorbing dichroic beamsplitters split the beam into different wavelength bands with high efficiency. The wavelength range of each channel is listed in Table 2.

Another important engineering factor is that the whole ECLIPS instrument must fit into the allocated mass and volume to guarantee mission success. Figure 1 is a preview of the

**Table 2** Coronagraph and its modules overview.

	UV	VIS	NIR
Wavelength range (nm)	200–525	515–1030	1000–2000
Modules	Camera with filter wheel	Camera and IFS	IFS and HRS

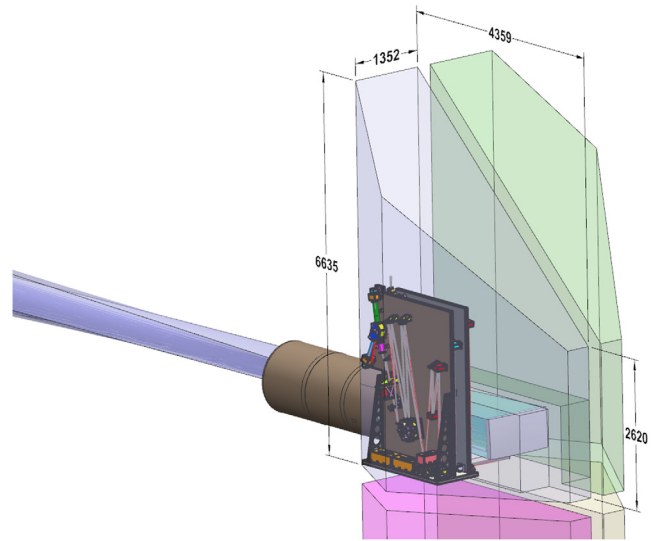


**Fig. 1** A preview of the ECLIPS instrument in the allocated volume.

ECLIPS instrument in the allocated volume. Large mechanisms that are used to select from multiple coronagraph masks and filters were especially challenging to accommodate. Table 3 shows a mass breakdown summary of the ECLIPS instrument. The initial maximum expected value (MEV) mass allocation of 1073 kg was derived from a mass budget of the entire LUVOIR observatory consistent with a Space Launch System Block 2 launch vehicle’s lift capacity. The mass budget was based on analogous systems, systems-engineering rules-of-thumb, and calculations of structure-to-supported-mass ratios. After detailed optical, mechanical, thermal, and electrical designs of the ECLIPS instrument were completed, the actual estimated MEV mass of the instrument is 963 kg. It is clear from the breakdown that the optomechanical assembly is the largest mass driver of the instrument. Minimizing the optical volume of the instrument is the most direct way to minimize the mass of the instrument,

**Table 3** An initial mass allocation for the ECLIPS instrument was derived from an observatory mass budget. The estimated mass is shown, along with a subsystem breakdown, after detailed optical, mechanical, thermal, and electrical designs were completed. The MEV is shown, which includes the estimated system mass, plus an additional 30% mass growth allowance to reflect the relatively low maturity of the designs. The additional mass margin is held at the observatory system level.

Initial mass allocation (MEV)	1073	kg
Total estimated mass (MEV)	963	kg
Optomechanical assembly	594	kg
Nonoptical structure	74	kg
Main electronics boxes	37	kg
Control system processors	29	kg
Thermal management system	91	kg
Harnessing	91	kg
Miscellaneous hardware	47	kg

and so, an effort to make the instrument as compact as possible was undertaken while still maintaining necessary imaging relationships between pupil and focal planes. The resulting optomechanical design not only achieved the mass allocation with margin but also fit within the available instrument volume, as shown in Fig. 1.

In the following sections, the optical design of the coronagraph and its instruments will be discussed in detail. Based on the two LUVOIR telescope designs (obscured versus unobscured), ECLIPS will use two possible coronagraph architectures: an apodized pupil Lyot coronagraph<sup>5-7</sup> (APLC) for the 15-m obscured telescope (LUVOIR-A) and a vector vortex coronagraph<sup>8</sup> (VVC) for the 8-m unobscured telescope (LUVOIR-B).

It is interesting to note that regardless of the telescope design and aperture size, the ECLIPS instrument performance requirements are the same. Furthermore, the first-order optical design requirements are driven not by the telescope aperture size, but rather by constraints placed on the pupil and image planes internal to the ECLIPS instrument. For example, the pupil plane diameters are driven by the size of available DMs and fabrication limitations on apodizing and Lyot masks. Similarly, the focal ratio of internal image planes is driven by fabrication limitations of the focal plane masks (FPMs). Imaging and spectral resolution of the back-end cameras are also identical between the two architectures, derived from top-level science requirements. Therefore, the optical design of the ECLIPS instrument for LUVOIR-A is nearly identical to that of ECLIPS for LUVOIR-B. The primary difference is in the first few preoptics that pick-off the beam from the telescope focal plane and relay it into the instrument module. Once an optomechanical design of ECLIPS for LUVOIR-A was completed, the design was ported to the LUVOIR-B model with only minor modifications to the preoptics.

This paper is organized as follows: Sec. 2 discusses the coronagraph and its three channels. Section 3 discusses the IFS designs for optical and NIR channels. Section 4 discusses HRS of the NIR channel. Section 5 discusses the cameras of the UV and optical channels. In each section, we connect the module specification to the ECLIPS top level requirement. A summary is provided in Sec. 6.

## 2 Coronagraph

In order to meet the top-level requirement of  $10^{-10}$  contrast, the coronagraph optical system is designed to provide a number of key surfaces for inserting coronagraph masks. To achieve starlight suppression with either an APPLC or a VVC, four critical planes must exist for inserting the masks: (1) a pupil plane for placing a deformable mirror (DM) for wavefront control; (2) a pupil plane for placing an apodization mask; (3) a focal plane for placing a FPM; and (4) a third pupil plane for a Lyot stop. Simulations have shown that with such a coronagraph optical system and specially designed APPLC masks,  $10^{-10}$  contrast can be achieved.<sup>9,10</sup>

As mentioned before, the ECLIPS coronagraph is designed in such a way that all three channels operate simultaneously to minimize the observation time and to see the activities of events for the full wavelength range at the same time.

### 2.1 Coronagraph Requirement

Achieving high contrast requires that the optical design is diffraction-limited at the shortest wavelength in each channel, and

**Table 4** DM and coronagraph masks for the study.

DM	50 × 50 mm	128 × 128 elements	Reflective (MEMS)
Apodization masks	100 mm diameter	10- $\mu$ m pitch	Reflective type
FPMs	Variety of sizes as function of $\lambda$	$f/15$ beam at mask	Transmissive type
Lyot stop mask	~20 mm diameter	NA	Transmissive type

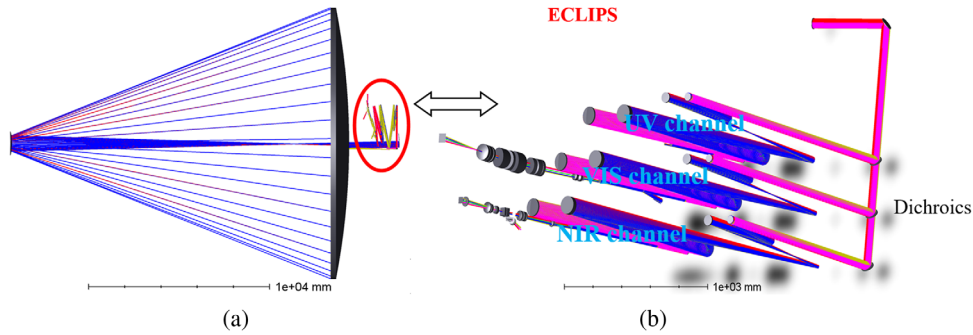
at each of the coronagraph mask planes (apodizer, focal plane, Lyot). Fortunately, the field-of-view (FoV) of the coronagraph is small ( $<1$  arc sec), so this performance can be achieved using simple off-axis parabola (OAP) mirrors only. The rest of the optical design requirements are driven by the hardware. For example, the size of the pupil in the DM planes is driven by the number of actuators across the DMs and their pitch. Similarly, the minimum manufacturable feature size of the apodization mask, focal plane, and Lyot masks are limited by today's state-of-the-art fabrication capabilities and constrain the plate scale of these beams. The parameters of the DM, apodization, and Lyot stop masks are listed in Table 4.

### 2.2 Coronagraph Optical Design

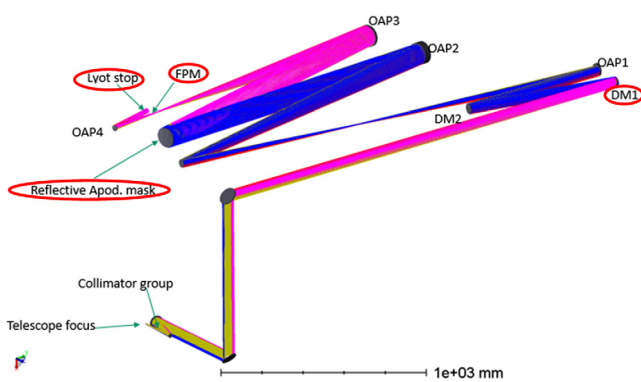
The key for the coronagraph design is to provide either pupil image or intermediate image planes for the masks in Table 4. Another key aspect of the coronagraph is to provide diffraction-limited performance in all planes over a minimum FoV  $32 \lambda/D$  and a preferred FoV  $64 \lambda/D$ . Figure 2 shows the coronagraph and its modules with the 15-m telescope. Both LUVOIR-A and LUVOIR-B are three-mirror anastigmats (TMA). The principal difference is that LUVOIR-B is an off-axis TMA to eliminate the central obscuration and its support structure.<sup>11</sup>

Figure 3 is the UV channel layout. The other two channels are the same as the UV channel up to the location of the spectral filters. The following is the list of each element and its functions. It also explains how the positions and sizes of the key elements are determined.

1. Collimator group: It includes two off-axis conic surfaces. Besides collimating the beam, it also relays the pupil images to DM1 with  $\phi$  (beam diameter)  $\sim 45$  mm. It is necessary to have DM1 in a pupil plane in order to correct wavefront errors (WFEs). The  $\phi \sim 45$  mm is less than DM's dimension of 50 mm.
2. DM1 and DM2 are selected as MEMS from Boston MicroMachines Co. They work with wavefront sensing mechanisms and coronagraph masks to obtain the designed high contrast. The distance between the two DMs is  $>800$  mm to allow for simultaneous correction of amplitude and phase. The minimum separation is driven by beam diameter and is a symptom of the Talbot effect<sup>7</sup> and how aberrations "mix" between phase and amplitude as the light propagates from the first DM to the second.



**Fig. 2** (a) On-axis 15-m LUVOIR TMA telescope and ECLIPS position relative to the telescope. (b) ECLIPS coronagraph channels and their modules. The three channels are split by dichroic beam-splitters in order to obtain the images from different channels simultaneously.



**Fig. 3** ECLIPS coronagraph optical layout. The labels with red circles are the four key coronagraph elements: DM1 and coronagraph masks. The figure shows that they are located at the four critical planes, as described in Sec. 2.

3. OAP1 and OAP2 collimate the beam and relay the pupil image to a reflective apodization mask. The collimated beam diameter needs to be  $\phi = 100$  mm to accommodate the minimum  $10\text{-}\mu\text{m}$  pitch size of the mask pattern.
4. The reflective apodization mask is a special design to create a high contrast FoV from  $4 \lambda/D$  to the required  $32$  (or preferred  $64$ )  $\lambda/D$ .
5. OAP3 focuses the collimated beam to an  $f/15$  beam to provide a focal plane for the FPM.
6. OAP4 collimates the beam again and provides one more pupil plane for the Lyot stop. A spectral filter wheel is just after the Lyot stop.

The collimated light after the Lyot stop and spectral filters is then relayed onto the back-end modules of each channel: each camera, the IFS, and HRS.

### 2.3 Coronagraph Performance

The coronagraph performance is measured by WFE. The analysis shows that the coronagraph is diffraction limited at all mask planes for the shortest wavelength of each channel, which is one of the requirements that is specific to the coronagraph optical design. Table 5 lists the WFE of each channel at the final

mask plane: the Lyot stop. The WFE is obtained using wavefront analysis tool in the optical design software Zemax, where all ECLIPS optics are designed and modeled. The maximum FoVs (half) for UV, optical, and NIR channels of a 15-m telescope are  $0.176''$ ,  $0.45''$ , and  $0.88''$ , respectively, which corresponds to  $64 \lambda/D$  at 200, 515, and 1000 nm, respectively. The maximum FoVs (half) of an 8-m telescope is  $0.330''$ ,  $0.850''$ , and  $1.650''$ , respectively. The definition of diffraction limited is that the WFE less than 0.071 waves, or  $\lambda/14$ . Table 5 shows that all WFEs are significantly better than the required 0.071 waves. It also indicates that there is plenty of room for the margin that includes fabrication and alignment tolerances.

The WFE in other mask planes, such as the DM, apodization mask, and FPM, is very similar due to the nature of pure reflective design for the coronagraph after the dichroic beam-splitter and due to the sub-arc-second FoV.

## 3 Integral Field Spectrographs

There is one IFS in the optical channel and one in the NIR channel. The spectrometers enable investigating the atmosphere of the targeted exoplanet to search for signs of habitability. Although each spectrograph has different performance requirements as determined by the different operational wavelength ranges, their optical configurations are similar. Both include relay optics, a lenslet-based field slicer, and refractive dispersing elements. The detailed specifications for both are detailed in Sec. 3.3. The main objective of the spectrometers is to provide enough resolving power to search for exoplanet biosignatures. The LUVOIR interim report indicates: “For planet characterization, we assume that  $\text{SNR} = 10$  on the planet continuum is required to constrain gas abundances, based on the results of spectral retrieval work using  $R = 140$  in the visible channel<sup>10,12</sup> and  $R = 70$  in the NIR. The  $R = 140$  spectral resolution in the visible is driven by the requirement to accurately characterize the O2 A-band and also to sufficiently retrieve H<sub>2</sub>O, O<sub>2</sub>, and O<sub>3</sub> abundances.<sup>10</sup> The NIR resolution is chosen to measure the broad NIR features like H<sub>2</sub>O and CH<sub>4</sub>. Note that LUVOIR-A also includes an option for  $R = 200$  in the NIR to resolve the narrow CO<sub>2</sub> feature near  $1.5 \mu\text{m}$ .”

The minimum requirements for each IFS are listed in Table 6. The preferred requirements are to have an outer working angle at  $64 \lambda/D$  for both telescopes and for all channels.

Even though the sampling at lenslet arrays and detectors is defined by the Nyquist criterion, they are driven by different requirements. The sampling at the lenslet array is a hard requirement to have a point source on the sky Nyquist sampled by the

**Table 5** Better than diffraction-limited WFE for all channels in Lyot stop plane for the best and worst FoV.

		WFE at central FoV (waves)		WFE at maximum FoV (waves)			
		15 m	8 m	15 m		8 m	
UV	$\lambda_{\min}$ 200 nm	0.01916	0.00330	0.03992	Max. FoV 0.176" (half)	0.01281	Max. FoV 0.330" (half)
	$\lambda_{\max}$ 525 nm	0.00730	0.00125	0.01521		0.00488	
Optical	$\lambda_{\min}$ 515 nm	0.00744	0.00128	0.03668	Max. FoV 0.45" (half)	0.01183	Max. FoV 0.850" (half)
	$\lambda_{\max}$ 1030 nm	0.00372	0.00064	0.01834		0.00551	
NIR	$\lambda_{\min}$ 1000 nm	0.00383	0.00066	0.01889	Max. FoV 0.88" (half)	0.00955	Max. FoV 1.650" (half)
	$\lambda_{\max}$ 2000 nm	0.00192	0.00033	0.00945		0.00477	

**Table 6** ECLIPS IFS requirement.

	Optical channel	NIR channel	Notes
Total bandpass	515–1030 nm	1000–2000 nm	From top-level requirement
Instantaneous bandpass	10%	10%	To obtain high contrast
Outer working angle at $\lambda_{\min}$ for $D = 15$ m	$32 \lambda/D$ (450 mas full)	$32 \lambda/D$ (880 mas full)	Prefer $64 \lambda/D$ . Limited by # of DM element.
Outer working angle at $\lambda_{\min}$ for $D = 8$ m	$32 \lambda/D$ (850 mas full)	$32 \lambda/D$ (1650 mas full)	Prefer $64 \lambda/D$ . Limited by # of DM element.
Optical throughput (end to end)	24% at 550 nm	48% at 1800 nm	Derived from yield.
Resolving power	140	70	From top requirement
Sampling at the lenslet array (based on the lenslet size)	Nyquist at 515 nm	Nyquist at 1000 nm	Postdata process requirement
Detector format	Electron-multiplying CCD (EMCCD) 4 k × 4 k 12- $\mu$ m pitch	H4RG 4 k × 4 k 10- $\mu$ m pitch	Derived from FoV and $R$

number of lenslets. Sampling at the detector is driven by the image of each spot formed by a lenslet and filtered by a pinhole on the back of the lenslet array to be Nyquist sampled by the detector pixels. Since the Lyot stop in both LUVOIR-A and LUVOIR-B are constrained to be the same size, IFS designs can be shared for both observatory concepts. The only difference is the plate scale, where the FoV on sky has a ratio of 8:15 for 15- and 8-m telescopes, respectively.

### 3.1 Lenslet Array Design

The main goal of the lenslet array design is to provide enough spacing among adjacent lenslets to display the spectral traces to satisfy the cross-talk requirement. It depends on the following parameters: (1) Spectral resolving power  $R$  and instantaneous bandpass  $\Delta\lambda$ , (2) cross-talk requirement, (3) magnification ratio of IFS collimator and imager, and (4) detector format and pixel size. The first two parameters are directly from ECLIPS top requirement and the rest of the result from optimizing IFS performance with currently available detectors.

To design the IFS, one must first design the lenslet array, because it determines the plate scale of IFS and its relay from Lyot stop of coronagraph to the lenslet array surface.

The specifications for the optimized lenslet shape and dimension are listed in Table 7.

To avoid difficulty in alignment and to increase the stability, a pinhole mask at the back surface of the lenslet array spatially

**Table 7** ECLIPS IFS lenslet array specification.

	Optical channel	NIR channel
Shape	Square	Hexagon
Lenslets size (side to side, $\mu$ m)	124	120
Material	Fused silica (Corning 7980)	Fused silica (Corning 7979)
Effective focal length (EFL) (mm)	0.992	0.96
Substrate thickness (mm)	1.426	1.394
Pinhole diameter ( $\mu$ m)	30	40
Lenslet array size (mm)	40 × 40	44 × 44

filters the lenslet images. Because of the shorter wavelength and the volume constraint, the optical IFS has a magnification ratio of 1:1.6 from the collimator to the imager. Therefore, even though the optical channel IFS has a higher resolving power  $R = 140$ , the lenslet size is not much larger than  $R = 70$  NIR IFS. For the lenslet material, the optical channel uses UV grade Corning 7980 or equivalent, and the NIR channel uses IR grade Corning 7979 or equivalent to avoid an absorption dip introduced around 1300 nm. The spherical lenslet surfaces are on the front surface of each lenslet array. The spherical surface might introduce some spherical aberration, but the spherical aberration is proportional to  $r^4$ , where  $r$  is the radius of the lenslet aperture. For all lenslets, the radius at the corners is less than  $100 \mu\text{m}$ , the aberration is tiny and, therefore, can be ignored. For example, the WFE of the rectangular lenslet array at  $\lambda = 615 \text{ nm}$  is 0.0021 waves RMS for spherical lenslet, which is only 3% of diffraction-limited 0.071 waves. If a conic surface is used for optimization, the WFE only improves slightly to be 0.0020 waves RMS.

Figures 4(a) and 4(b) show the lenslet geometry of the optical and NIR channels, respectively. The length of the spectral traces of 34 pixels for the square lenslet array is to meet the spectral resolving power of  $R = 140$  plus the 4-pixel separation between any two adjacent traces in one line. The length of 20 pixels for the hex lenslet array is to meet the spectral resolving power of  $R = 70$  plus separation between traces. A few more pixels are also included to deal with the slight nonuniformity of spectral resolving power due to compound prisms, which will be discussed in Sec. 3.3.

The lenslets of both optical and NIR channels were modeled in the optical design software ZEMAX. They are shown in Fig. 5.

### 3.2 Relay Optics for IFS

With the calculated lenslet size, it is ready for relay optics design. The main function of the relay optics is to magnify the image onto the lenslet array to meet the Nyquist requirement at  $\lambda_{\text{min}}$  for both the optical and NIR channels. The specification of the relay is listed in Table 8. The notes in the last column indicate where the numbers are derived from.

An off-axis Cassegrain telescope was selected for the relay. A single OAP can also provide diffraction-limited performance for such a small FoV. Both designs are virtually aberration free.

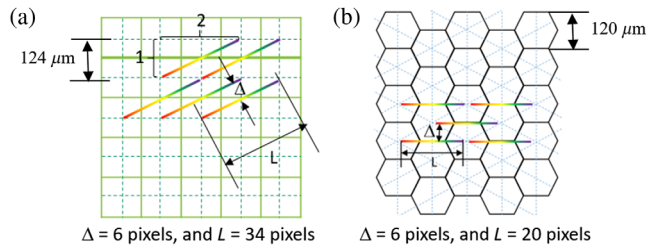


**Fig. 4** ECLIPS IFS lenslet geometry in XY plane. (a) Square lenslet array for optical IFS. The square lenslet size (side to side) is  $124 \mu\text{m}$ . With 1:1.6 magnification from lenslet array to detector array, the length of each spectral trace is 34 pixels on the detector array, and the separation in nondispersion direction is  $\Delta = 6$  pixels to avoid cross-talk. (b) Hexagon lenslet array for NIR IFS. The hex lenslet size (side to side) is  $120 \mu\text{m}$ . With 1:1 magnification from lenslet array to detector array, the length of each spectral trace is 20 pixels on the detector, and separation in nondispersion direction is also  $\Delta = 6$  pixels.

However, the focal length of a single OAP for the optical and NIR channels must be 9.7 and 5.0 m to meet the required  $f/\# = 481.5$  and 248 for required point spread function (PSF) sampling, respectively. This causes problems for packaging into an allocated volume. Therefore, the more compact off-axis Cassegrain telescopes are used as the relay telescopes for both channels. The layout of the relay for the optical channel is shown in Fig. 6. The optical relay mirror (ORM1) and ORM2 are the primary mirror and secondary mirrors, respectively. Even though the magnification and  $f/\#$  of the NIR relay are different from the optical relay, the layout looks very similar. It is not shown here.

The optical performance at the lenslet array is diffraction limited for both channels and both 15- and 8-m telescopes. Because the relay is virtually aberration free, the WFE is very similar to the WFE listed in Table 5. Even though the required minimum IFS FoV is  $32 \lambda/D$ , the diffraction-limited performance is over the entire preferred  $64 \lambda/D$  FoV for the entire wavelength range.

### 3.3 IFS Optical Design and Performance

Three candidate spectrographs were based on lenslets, an image slicer, and lenslet + fiber. Among them, the lenslet-based IFS was selected for the LUVOIR study because of its simplicity, and its capability to provide high throughput and high spatial resolution. For the other two IFS types, the image slicer is not able to provide the desired spatial resolution, and the throughput loss from the lenslet array to a single mode fiber makes it unfit for exoplanet applications. Based on the latest and advanced image slicer design from Wide-Field Infrared Survey Telescope (WFIRST) integral field channel design, the smallest slice width is 0.25 mm, and the total number of slices is only 20.<sup>13</sup> Even though the number of slices could be doubled, or even tripled, to achieve the 256 slices that are needed to obtain Nyquist sampling for  $64 \lambda/D$  FoV is still beyond current capabilities. Besides, the optics between slicer and spectrometer are also a great challenge, requiring an array of 256 pupil mirrors and 256 slit mirrors to match the number of the slices. That is, the more slices it has, the more difficult the design, alignment, and stability requirements are.

The main problem of the lenslet + fiber design is the low coupling efficiency between a lenslet and a single-mode fiber. When we need to couple laser light into a single-mode fiber, we move from the geometric ray trace to a Gaussian mode-matching problem.<sup>14</sup> Even to couple monochromatic visible light from a laser diode into a single-mode fiber is not trivial. In theory, the coupling efficiency of the single mode fiber depends on how well the incident optical wavefront matches the output Gaussian beam from the single mode fiber. Any mismatch, such as a non-Gaussian beam, misalignment, etc. will end up with coupling efficiency reduction. For example, even though a lenslet array does not have gaps as packed fiber tips, but the mismatch to the Gaussian beam from fiber makes the area advantage of no-gap lenslet array disappear because the light from the corners of the lenslet does not match the Gaussian mode of the fiber. A more significant loss is the wide wavelength range of both the optical and NIR channels. The lenslet design can only be optimized to match one wavelength, for other wavelengths in the range, the coupling efficiency will decrease due to a mismatch between PSF and fiber core size. In practice, to accurately align more than 70,000 fibers both positionally and angularly with such a tight tolerance is probably the most challenging part to obtain the high coupling

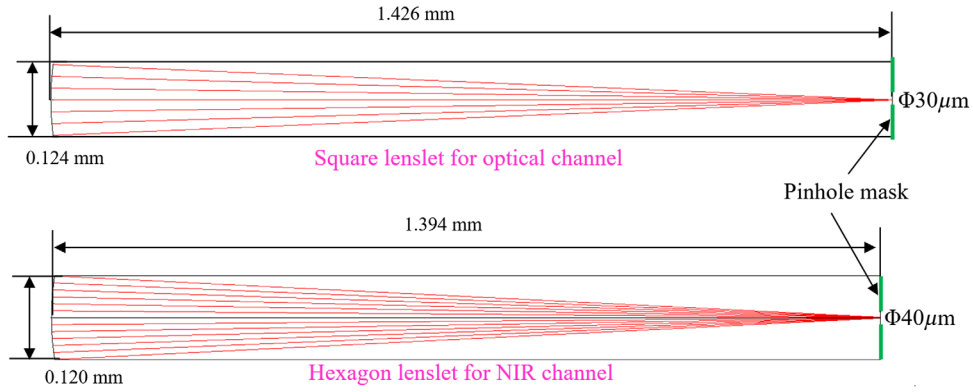


**Fig. 5** The single lenslet ray trace in the cross-section. In this design, the focus is designed right at the back of the lenslet array substrate, where a pinhole make is deposited on. The core of the diffraction limited PSF passes the pinhole, most of the ring structure and of the PSF and stray light are blocked by the pinhole to improve the contrast. Based on the wavelength and plus the tolerance, the pinhole diameter for optical lenslet array is  $30\ \mu\text{m}$ , and for NIR lenslet array is  $40\ \mu\text{m}$ . The full lenslet array in optical channel includes 72,300 square lenslet and that in NIR channel 128,000 hexagon lenslets.

**Table 8** ECLIPS IFS relay specification.

	Opt. channel	NIR channel	Notes
Wavelength range (nm)	515–1030	1000–2000	Wavelength limitation of detector, lens, coating, etc.
EFL (m) (with telescope)	7704	3968	To meet Nyquist sampling
EFL (m) (relay alone)	9.735	5.015	To meet Nyquist sampling
$f/\#$ at lenslet array	481.5	248	Calculated
Lenslet shape	Square	hexagon	Optimize detector pixel efficiency
Incident beam diameter (mm)	20.22	20.22	Lyot stop size
Total # of lenslets	72,300	128,000	Calculated

efficiency. In the estimate, the throughput will be less than 50% compared to the lenslet array alone. It should be mentioned that a new type of fiber, photonic crystal fiber, could support single mode for broad wavelength range with a relatively larger core

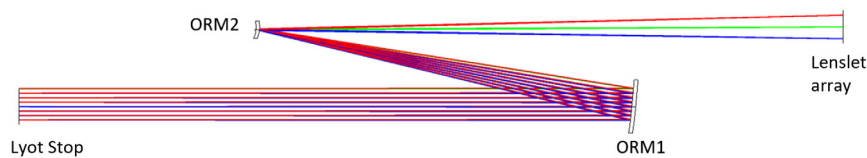
size ( $\sim 10\ \mu\text{m}$  with low throughput loss in optical range). However, the numerical aperture from the lenslet is the same for all wavelengths, and the PSF size is still a function of the wavelength. So, no real advantage from theoretical coupling efficiency is gained, but it might relax the alignment tolerance a little.

After the IFS type was selected, the next step was to design a spectrometer. A prism type spectrometer is needed for the lenslet based IFS unless the wavelength range of the spectrometer is only a small portion of the grating free spectral range, and the FoV is small enough to push the unwanted diffraction orders out of the detector array. The design specifications derived from the optical and NIR IFS requirements are listed in Table 9. Both use a pure refractive design with compound prisms for the spectrally dispersive element. Both of them have a collimator group and an imager group with compound prisms in between. However, they are different enough and will be discussed separately.

### 3.3.1 IFS for optical channel

From an optical design point of view, the design for the IFS in the optical channel is quite challenging due to the following reasons: (1) It requires a higher spectral resolving power; (2) the dispersion of glass material is much higher at shorter wavelengths than at longer wavelengths, so chromatic aberration is more difficult to control; (3) relatively large detector size;

## Optical Channel Relay



Note: Each color represents rays from each field. It is not a diverge beam. Beam from each field focuses on the lenslet surface with a very large  $f/\#$ .

**Fig. 6** The optical channel relay design provides a focus of  $f/481.5$  beam onto the surface of the lenslet array for making the full width half max (FWHM) of the point spread function (PSF) meet the Nyquist sampling at  $\lambda = 515\ \text{nm}$ .

**Table 9** Specification for optical and NIR IFSes.

	Optical IFS	NIR IFS
Wavelength range (nm)	515–1030	1000–2000
Instantaneous bandpass	10%	10%
Magnification (object: image)	1: 1.47	1: 1
$f/\#$ after lenslet (side to side)	8	8
$f/\#$ at detector (side to side)	11.76	8
Spectral resolving power (R)	$140 \pm 10$	$70 \pm 10$
Spatial sampling	Meet Nyquist at $\lambda_{\min}$	Meet Nyquist at $\lambda_{\min}$
Object size (mm)	$33.28 \times 33.28$	$40 \times 40$
Total spectral length (detector pixels)	34 (include isolation pixels)	20 (include isolation pixels)
Cross dispersion separation (pixels)	6	6
Detector	EMCCD 4 k $\times$ 4 k, 12- $\mu\text{m}$ pitch	H4RG 4 k $\times$ 4 k, 10- $\mu\text{m}$ pitch

and (4) mass and volume limit. To overcome these challenges, the optical IFS design chose a magnification of 1:1.47 between object and image, instead of commonly used 1:1. In other words, the collimator group and the imager group have different focal lengths.

The IFS is designed to use the maximum circular area of the selected detector chip, even though the outer working angle of  $64 \lambda/D$  (as limited by the number of actuators across the DM aperture) is smaller than this. This is because there are nonhigh contrast science cases that may use the coronagraph IFS to obtain spectra over the larger FoV. With the 1:1.47 magnification, the object size reduces  $\sim 1/3$ , which not only makes the aberration easier to control but also reduces the size of the collimator. On the other hand, the 6 pixels of cross-dispersion separation can easily handle the Airy disk size at the longest wavelength of 1030 nm for an  $f/11.76$  beam.

With the Nyquist sampled PSF overfilling the individual lenslet, the real aperture stop, in this case, is the lenslet boundaries, either square or hexagonal. In the standalone IFS model, it is important to make sure that the  $f/\#$  of the object equals the  $f/\#$  of the designed lenslet, and the chief ray directions follow the chief ray directions of relay optics for the entire FoV. The optical IFS design is optimized using the ray trace software Zemax. The layout of the design is shown in Fig. 7. The spot diagram is shown in Fig. 8. The spectral resolving power versus wavelength is shown in Fig. 9. It is seen that the spectral resolving power is not perfectly flat but meets the  $R = 140 \pm 10$  requirement. With the limitation of available materials, for providing high transmittance for the entire wavelength range, it is hard to make it perfectly flat. But if more time has been spent to optimize the combination of glass material dispersions and prism apex angles, improvement is definitely possible. It is also worthwhile mentioning that the spectrometer design provides the dispersion for the full wavelength range. However, only an instantaneous band (10%) is observed at any particular time. All spectral traces shift on the detector for different instantaneous bands, but they never overlap for any instantaneous band as long as the bandwidth of the spectral filters does not exceed 10%. It should also be pointed out that the compound prism does not provide zero deviation at the central wavelength. This is due to the trade to have the spectral resolving power flatter than to have zero deviation. Zero deviation has some advantage during alignment, but we have shown that a nonzero deviation IFS can be aligned precisely using optical model and metrology tools for a prototype IFS “PISCES” for WFIRST coronagraph testbed.<sup>15,16</sup> At last, it should be pointed out that for the optical channel, the detector is mounted to a detector housing with a fold mirror in front to reflect the light into the EMCCD. This is due to the concern that high energy particles will add noise and degrade the detector performance over time, as studied by the WFIRST coronagraph instrument (CGI).<sup>17</sup> The housing and fold mirror will limit the solid angle of this light to hit the detector in two ways: (1) In order to mount a relatively large detector housing, the field corrector has to be removed, which makes the optical path length from the last optical element to detector significantly longer. Compared to the NIR IRS in Sec. 3.3.2, the ratio of the solid angle of NIR to optical IFS is 8:1. (2) Comparing with and without detector house for the CCD at the same distance from the last optical element, the solid angle reduction is  $\sim 4:1$ . For most of the applications, this may not be a problem. But the exoplanet detection requires such high contrast, every effort has been made to retire as much potential risk as possible to improve the SNR.

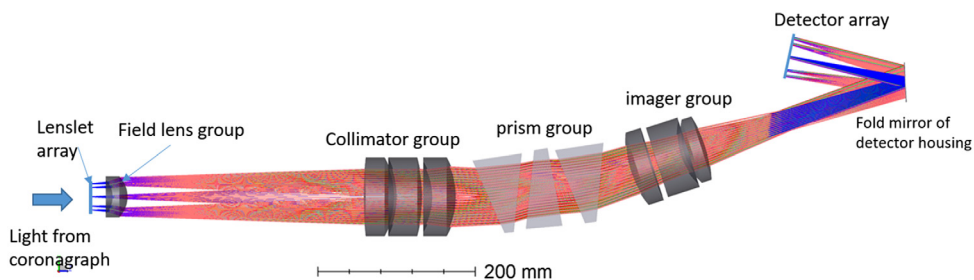


**Fig. 7** Optical IFS design. The field lens is used to control the chief rays to reduce the diameter of the collimator group. The compound prisms are to provide the required spectral resolving power. Meanwhile, the material selection of three prisms is for making the spectral resolving power as flat as possible in the defined wavelength range.

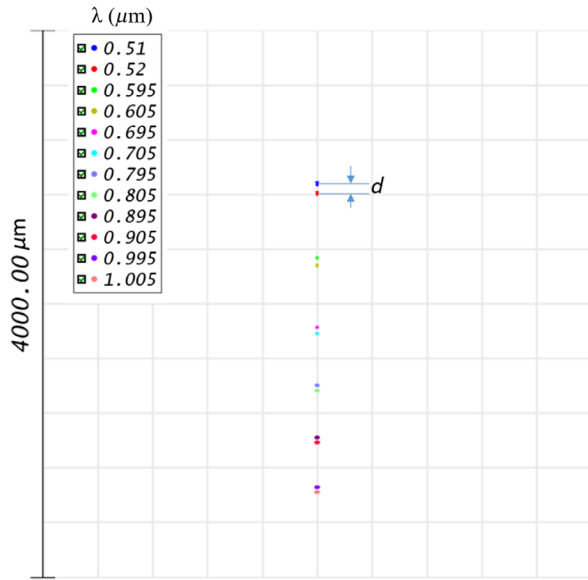


**Fig. 8** The spot diagram at detector array for full wavelength range at the central FoV. The box on the upper-left corner indicates the wavelength in microns of each spot. The wavelength separation of each pair of spots is 10 nm. The physical separation  $d$  on detector array is calculated by Zemax ray trace.

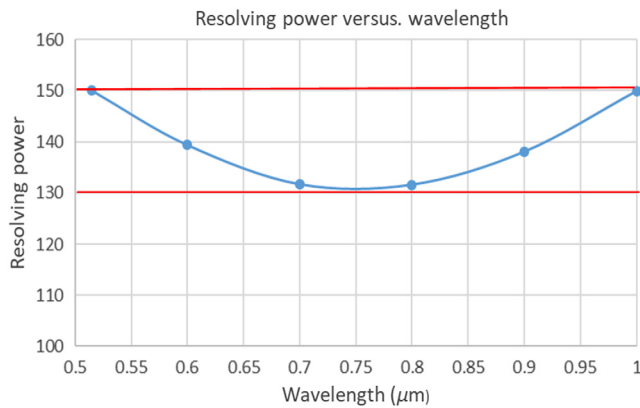


**Fig. 9** Spectral resolving power meets the required  $R = 140 \pm 10$ . Two red lines are the bonding lines for required spectral resolving power. Resolving power is defined by  $R = \lambda/\Delta\lambda$ . The data points are calculated from traced spots shown in Fig. 7. For each pair of spots in Fig. 7, the  $\lambda$  used for computing  $R$  is the mean of the two wavelengths.  $\Delta\lambda$  is the wavelength separation to be resolved for two detector pixels (Nyquist). For example, the ray trace in Fig. 7 provides  $d$  for 10-nm wavelength separation, the pitch of the selected detector is  $\delta$ , then  $\Delta\lambda = (2 \times 10)/(d/\delta)$  nm, where  $d$  and  $\delta$  are in the same unit.

### 3.3.2 IFS for NIR channel

The optical design for the NIR IFS is relatively easier because the spectral resolving power is only  $R = 70$ . Besides, the glass dispersion for longer wavelengths is lower, and the detector size is a little smaller at  $40 \times 40$  mm. So, the magnification for the NIR IFS is kept at 1:1. It is seen that the compound prisms generated less beam deviation than the optical channel due to the lower spectral resolving power  $R = 70 \pm 10$ . Also, the number of prisms reduces to two. It should be mentioned that two prisms make the resolving power less flat over the full spectral band, although it still meets the specification. Of course, the glass material selection for the two channels is very different. For the optical channel, the high transmittance materials from 515 to 1030 nm are selected, and for the NIR, those from 1000 to 2000 nm are selected. Because the luminescent or fluorescent light is mainly in the shorter wavelength range, the H4RG detector is not sensitive in that range. Therefore, the fold mirror in front of the detector is no longer needed. The optical layout and the resolving power are shown in Figs. 10 and 11.

## 4 High-Resolution Spectrometer

The HRS is only in the NIR channel. The function of the HRS is to provide high spectral resolution to investigate the detail of the spectrum for the interested exoplanets observed by the NIR IFS. The HRS specification is listed in Table 10.

The HRS and NIR IFS share the same collimator optics (see Fig. 12). Two mechanisms are designed for the HRS: a slit before the NIR lenslet array and a flip fold mirror right after the collimator. When an interesting exoplanet is found, a steering mirror in the HRS relay optics is used to move the exoplanet to the center of the lenslet array. Then, the slit is moved in to limit the instrument FoV to just the exoplanet. After the exoplanet spectrum is shown in the IFS, the fold mirror is flipped in to direct the beam to the HRS. The HRS consists of two prisms and an imager lens group. A trade has been performed between a prism and a grating as the HRS dispersive element. The prism is selected because of the following reasons: (1) the required resolving power  $R = 200$  is comfortable for the prism to handle. In the case of having prisms in collimated space, the resolving power is proportional to the product of angular dispersion of prism and the focal length of the focusing optics. The focal length of the HRS focusing optics is close to 300 mm, to obtain  $R = 200$  the prism only needs to provide a dispersion of 0.5 deg for the total wavelength range of 1000 nm, which is in prism's comfort zone. (2) The prism provides higher throughput over the full wavelength range. For the alternative gratings, the diffraction efficiency is high at the peak wavelength but drops gradually toward the edge wavelengths to 70%<sup>18</sup> of the peak in our wavelength range, which is the full free grating spectral range from 1000 to 2000 nm. Since each channel uses a number of

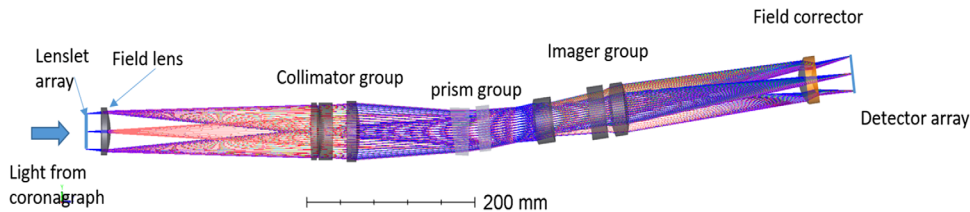


**Fig. 10** NIR IFS design. The field lens is used to control the chief rays to reduce the diameter of the collimator group. Two prisms are used to provide the required spectral resolving power and required flatness.

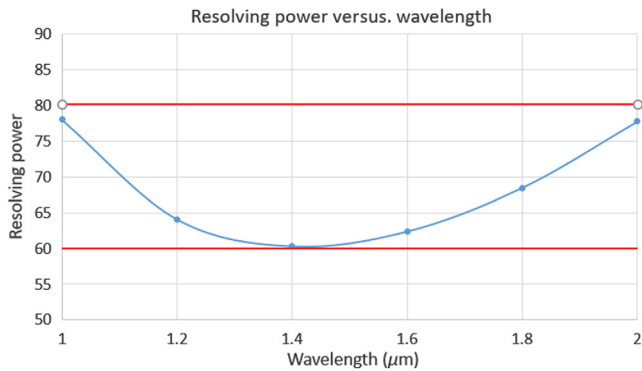


**Fig. 11** Spectral resolving power of the NIR IFS. The plot shows that resolving power meets the specified  $R = 70 \pm 10$ . It is calculated using the same way as for the optical channel.

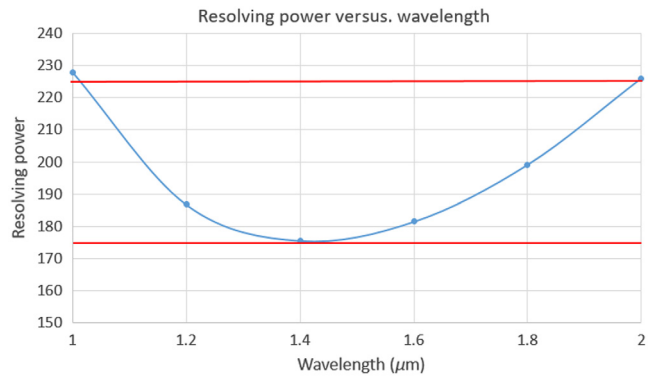


**Fig. 13** Spectral resolving power of NIR HRS meets the required  $R = 200 \pm 25$ .

**Table 10** Specification for the NIR HRS.

Wavelength range (nm)	1000–2000
$f/\#$ side to side	8
Spectral resolving power	$R = 200 \pm 25$
Spatial resolution	Diffraction limited at $\lambda_{\min}$
Object size (mm)	$6 \times 6$ (slit position in this area)

spectral filters with 10% of bandpass, at the bands of two edges, the throughput drops to 30%. As a result, the exposure time needs to be 30% longer to achieve the same SNR. (3) No unwanted orders or orders overlap of the spectrum. (4) The grating provides a constant spectral resolution but not resolving power. When the detector pixel size is included, the spectral resolving power provided by the grating increases with wavelength.

The resolving power for the HRS is plotted in Fig. 13.

## 5 Cameras for UV and Optical Channels

The specifications for the UV and optical cameras are listed in Table 11. Their designs are relatively straight forward compared to the IFSes and the HRS. They are similar to the relay optics for IFSes but have different magnifications to meet Nyquist sampling requirements at the detector. The main requirement for cameras is to provide diffraction-limited performance. Even though the diffraction-limited performance looks the same

**Table 11** Camera specifications for the UV and optical channels.

	UV	Optical
Wavelength range (nm)	200–525	515–1030
Sampling at detector	Nyquist at 200 nm	Nyquist at 515 nm
Pupil diameter (mm)	20.22	20.22
$f/\#$	130	50.48
EFFL (mm)	2628.2	1020.8
RMS WFE	Diffraction limited	Diffraction limited
FoV	$32 \lambda/D$	$32 \lambda/D$
Detector array	1 k × 1 k with 13- $\mu$ m pitch	1 k × 1 k with 13- $\mu$ m pitch

throughout ECLIPS instrument, the diffraction-limited performance at UV (200 nm) is much more challenging than that in visible and NIR wavelength range. Therefore, the off-axis Ritchey Criterion Telescope is used for the camera relay optics. Compared to the IFS relays, the  $f/\#$  of the cameras are relatively small at  $f/130$  and  $f/50.48$  for the UV and optical channels, respectively. This is benefitted from much smaller detector pixel size than lenslet size. The WFE requirement after Lyot stop is not as critical, because the starlight suppression for high contrast is already completed at this point. However, the diffraction-limited performance is still required to keep the

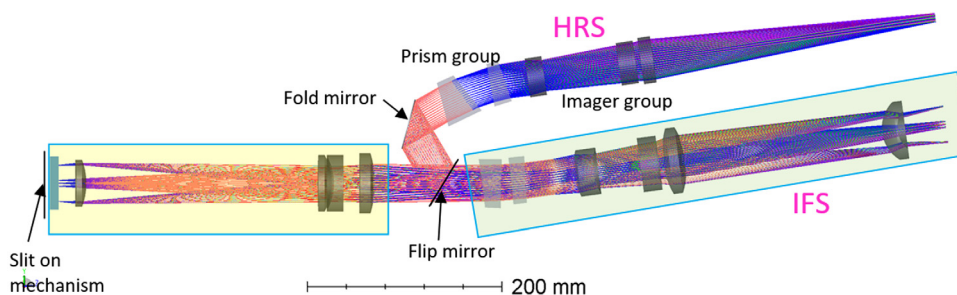


**Fig. 12** NIR HRS design. A flip in and out mirror with a mechanism is used to switch between the NIR IFS and the HRS. The additional fold mirror in the HRS channel is just used for packaging.

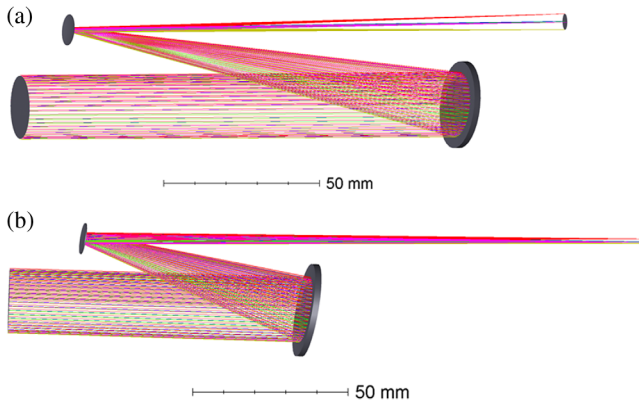


**Fig. 14** Coronagraph cameras for UV and optical channels: (a) UV camera and (b) an optical camera.

maximum power in the Airy disc for increasing exoplanet detection yield. Actually, we would like to keep the design residual as low as possible to provide room for fabrication, alignment, and environmental errors. The UV channel does not have a spectrometer. The layout of both cameras is shown in Fig. 14.

The performance of the cameras is evaluated by WFE, as are most astronomical applications. Figures 15 and 16 show the WFE mapping for cameras of the UV and optical channels. The diffraction-limited wavefront is 0.071 waves. The maximum scale of the maps is 0.05 waves, which indicates that the performance of the entire FoV is diffraction limited. Compared to the WFE at Lyot stop that is listed in Table 5, the difference is minimal except the upper right corner of 200 nm for 15-m telescope. That means the WFE of standalone cameras is minimal, and cameras are well designed.

Only the shortest wavelength in each case is shown. The WFE for longer wavelengths (measured in waves) is inversely

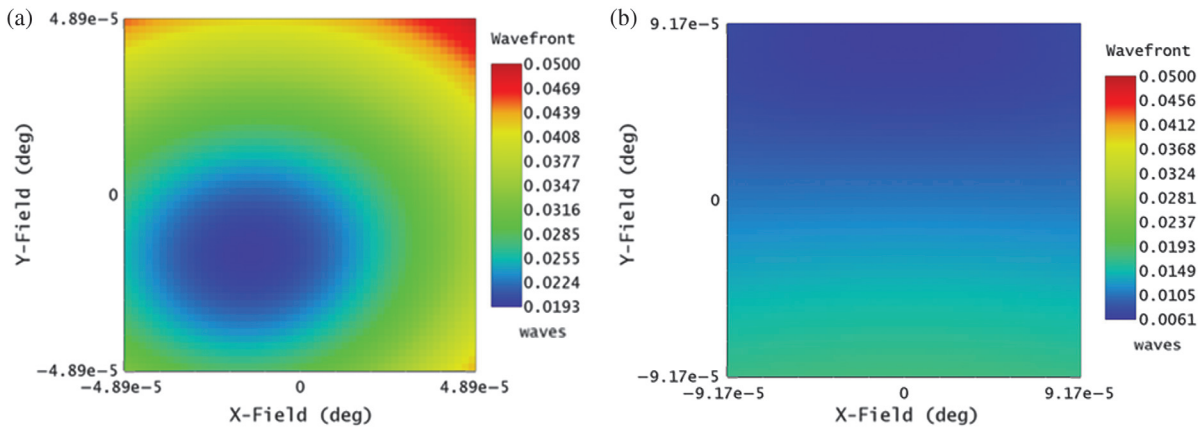


**Fig. 15** The WFE maps for the UV camera at the shortest wavelength  $\lambda = 200$  nm. The color bar is in waves of 200 nm. It shows that the WFE requirement is met with plenty of margins. (a) The map on the left is for the 15-m telescope and (b) the map on the right is for the 8-m telescope. Both maps have a FoV of  $64 \lambda/D$ . The correspondent FoV on the sky is  $0.352''$  and  $0.660''$  for the 15 and 8 m, respectively. It is noted that the performance for 8 m is much better than that for 15 m. The difference is mainly due to the residual telescope WFE for 15 m is higher than 8 m. Camera alone is almost aberration free.

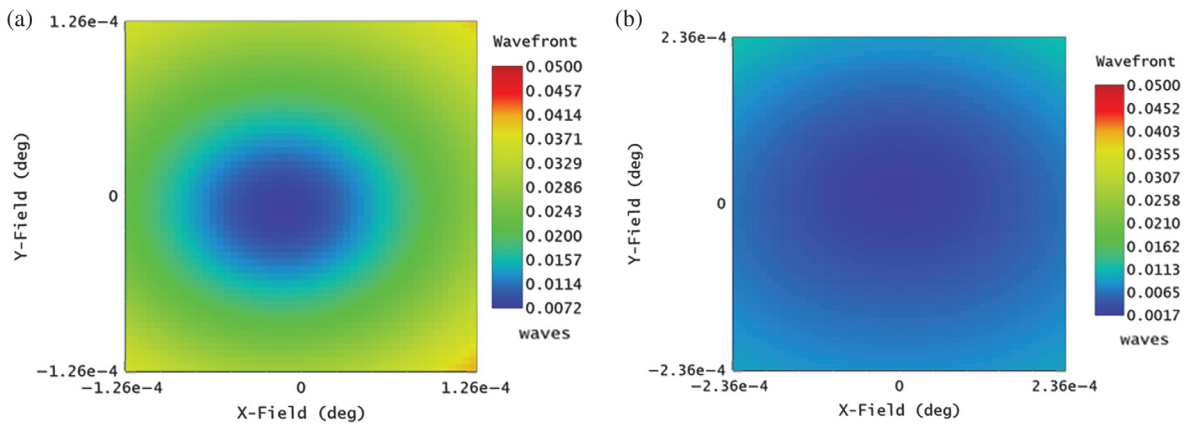


**Fig. 16** The wavefront map for the optical camera at the shortest wavelength  $\lambda = 515$  nm. Compared to UV channel, it meets the requirement with an even larger margin. The color bar is in waves of 515 nm. (a) The map on the left is for the 15-m telescope and (b) the map on the right is for the 8-m telescope. Both maps have a FoV of  $64 \lambda/D$ . The correspondent FoV on the sky is  $0.906''$  and  $1.700''$  for the 15 and 8 m, respectively. Same as in Fig. 14, the difference of the WFE for 15 and 8 m is mainly due to the residual aberration difference from telescope designs.

scaled down. This is because in the whole camera path, from the telescope to the coronagraph to the cameras, all optical elements are reflective. The absolute WFE measured in nanometers (or other length units) is the same. When scaled to the wavelength to evaluate if it is diffraction limited, the longer the wavelength is, the smaller the WFE.

## 6 Summary

The ECLIPS optical system for both the 15-m and 8-m telescopes has been designed and analyzed under the LUVOIR study for the 2020 Astronomy and Astrophysics Decadal Survey. The ECLIPS instrument is configured to have a coronagraph and five back-end modules: two IFSEs, one HRS, and two cameras, to achieve the top level requirement set by science goals. The specifications for each coronagraph and each module are described. The optical designs based on the derived specifications are presented, and performance is analyzed. The results show that all coronagraphs and the five back-end modules meet the specifications at all wavelengths, at all coronagraph critical planes, and at all cameras and spectrometers. That implies that the designed optical system has the capability to fully support the ambitious exoplanet exploration mission. During the optical design, the effort has been made to select as technically mature elements without compromising the required performance.

The ECLIPS design is interchangeable between the 15-m and the 8-m LUVOIR telescope designs. The only differences are as follows:

1. The first collimator in the coronagraph has a different prescription for the 15 and the 8 m. All designs other than that are identical.
2. The FoV is  $64 \lambda/D$  for both designs and is therefore different on the sky for each telescope. LUVOIR-A, with a 15-m aperture, has a smaller FoV on the sky and is, therefore, able to access more distant exoplanet systems.

Even though the required FoV is  $32 \lambda/D$  for the shortest wavelength of each channel, the preferred FoV of  $64 \lambda/D$  is used throughout the ECLIPS optical design to allow for a potentially more-capable instrument that should have the required DM and detector technologies be developed. All performance specifications are met for  $64 \lambda/D$ .

Finally, we would like to emphasize the unique advantages of a large telescope: The capability to detect the Earth-sized exoplanets very close to Sun-like stars and the enhanced capability of a large telescope's photon collecting power enables spectral analysis to search for biosignatures and to determine if the detected exoplanet is habitable.

## Acknowledgments

The LUVOIR Study would like to acknowledge its sponsors: NASA HQ, Science Mission Directorate, Astrophysics Division, and NASA's Goddard Space Flight Center.

## References

1. M. R. Bolcar et al., "The large UV/optical/infrared surveyor (LUVOIR): decadal mission study update," *Proc. SPIE* **10698**, 106980O (2018).
2. A. Wolszczan and D. A. Frail, "A planetary system around the millisecond pulsar PSR1257 + 12," *Nature* **355**(6356), 145–147 (1992).
3. "The LUVOIR interim report," Pages Chapter 1 p. 2–3, Chapter 3–7, Chapter 2 p.16, 2018, [https://asd.gsfc.nasa.gov/luvoir/resources/docs/LUVOIR\\_Interim\\_Report\\_Final.pdf](https://asd.gsfc.nasa.gov/luvoir/resources/docs/LUVOIR_Interim_Report_Final.pdf)
4. C. C. Stark et al., "Maximizing the exoEarth candidate yield from a future direct imaging mission," *Astrophys. J.* **795**(2), 122 (2014).
5. M. N'Diaye et al., "Apodized pupil Lyot coronagraphs for arbitrary apertures. V. Hybrid shaped pupil designs for imaging earth-like planet with future space observatories," *Astrophys. J.* **818**(2), 163 (2016).
6. K. St. Laurent et al., "Apodized pupil Lyot coronagraphs designs for future segmented space telescopes," *Proc. SPIE* **10698**, 106982W (2018).
7. J. Mazoyer et al., "Active correction of aperture discontinuities—optimized stroke minimization II: optimization for future missions," *Astron. J.* **155**, 8 (2018).
8. G. Ruane et al., "Apodized vortex coronagraph designs for segmented aperture telescopes," *Proc. SPIE* **9912**, 99122L (2016).
9. R. Juanola-Parramon et al., "Evaluating the LUVOIR coronagraph sensitivity to telescope aberrations," in *IEEE Aerosp. Conf.* (2019).
10. L. Pueyo et al., "The LUVOIR architecture 'A' coronagraph instrument," *Proc. SPIE* **10398**, 103980F (2017).
11. G. J. West et al., "Optical design and status of the large ultra-violet optical infrared surveyor (LUVOIR)," *Proc. SPIE* **10698**, 6 (2018).
12. T. D. Brandt and D. S. Spiegel, "Prospects for detecting oxygen, water, and chlorophyll on an exo-Earth," *Proc. Natl. Acad. Sci. U. S. A.* **111**, 13278–13283 (2014).
13. G. Gao et al., "Optical design of the WFIRST phase-a integral field channel," *Proc. SPIE* **10590**, 105901R (2017).
14. J. Panigrahi, "Laser coupling efficiency in single mode fiber," PhD Thesis (2013).
15. Q. Gong et al., "Prototype imaging spectrograph for coronagraphic exoplanet studies (PISCES) for WFIRST/AFTA," *Proc. SPIE* **9605**, 96050G (2015).
16. M. W. McElwain et al., "PISCES: an integral field spectrograph technology demonstration for the WFIRST coronagraph," *Proc. SPIE* **9904**, 99041A (2016).
17. R. Effinger et al., "WFIRST coronagraph detector trap modeling results and improvements," *Proc. SPIE* **10709**, 1070917 (2018).
18. G. J. Swanson, "Binary optics technology: theoretical limits on the diffraction efficiency of multilevel diffractive optical elements," Lincoln Laboratory Technical Report 914, pp. 9–11 (1991).

**Qian Gong** is a research optical engineer at NASA Goddard Space Flight Center. She received her PhD from the Optical Sciences Center, University of Arizona, in 1990. She is on a Goddard research engineering partnership program to work with scientists for developing innovative concept design to achieve challenging science goals. Meanwhile, she also designed WFIRST grism and prism spectrometers and CGI integral spectrograph. Prior to that, she has worked on HST, JWST, and many other projects as an optical engineer or optics lead.

**Matthew R. Bolcar** is an optical system engineer at NASA's Goddard Space Flight Center. Currently, he serves as the lead engineer for the LUVOIR Decadal Mission Concept Study. He recently served as the chief technologist for the Advanced Technology Large Aperture Space Telescope (ATLAST) concept study. The additional projects that he has worked on include the thermal infrared sensor (TIRS) instrument on board LandSat 8, the Advanced Topographical Laser Altimeter System (ATLAS) instrument on board ICESat 2, the Visible Nulling Coronagraph, and the wide-field imaging interferometer testbed. prior to coming to Goddard, he received his BS degree in engineering physics from Cornell University in 2002 and earned his PhD under professor James R. Fienup at the University of Rochester in 2009.

**James A. Corsetti** is an optical engineer and member of the optical design group at the NASA Goddard Space Flight Center. He received both his BS and PhD degrees from the Institute of Optics at the University of Rochester.

**Julie A. Crooke** is the Astro2020 Decadal LUVOIR study manager. She also serves as NASA Goddard's Deputy Center chief technologist. She previously served as the astrophysics business development manager for ten years, and for fifteen years prior to that, she

was an optical systems engineer for Hubble's first servicing mission, Cassini's Composite Infrared Spectrometer (CIRS), ICESAT1's Geoscience Laser Altimeter System (GLAS), STEREO's Coronagraph1 (COR-1), and Spitzer's Infrared Array Camera (IRAC) and numerous technology and proposal efforts.

**Joseph Generie:** Biography is not available.

**Tyler D. Groff** received his bachelor's degree in mechanical engineering and astrophysics in 2007 from Tufts University and his PhD in mechanical and aerospace engineering from Princeton University in 2012. His research focuses on visible and near-infrared instrumentation for exoplanet science, coronagraph design, and wavefront control. He is the lead engineer at Goddard for the WFIRST CGI integral field spectrograph. Prior to working at Goddard, he was the laboratory manager of the Princeton High Contrast Imaging Laboratory, where he led the design, construction, and commissioning of the CHARIS integral field spectrograph for the Subaru telescope.

**Jason Hylan** is a mechanical engineer at NASA Goddard Space Flight Center and is currently the deputy lead engineer for the LUVOIR study engineering team. Prior to working on LUVOIR, he served as both the lead mechanical systems engineer for JWST's Integrated Science Instrument Module (ISIM) Element and the deputy manager for the integration and test of JWST's Optical Telescope Element and ISIM Element (OTIS) assembly.

**Andrew Jones** has been working as an aerospace engineer at NASA/Goddard Space Flight Center since 1985. He received his bachelor of science degree in mechanical engineering from the University of Maryland and his master's degree from Embry-Riddle. His work at NASA has covered a wide variety of structural and conceptual designs for spacecraft, instruments, experiments, and research and development projects in every stage of the mission timeline. Early work included many flight missions. Later work focused on conceptual designs for future missions and proposals including most aspects of the GSFC mission suite from facility class observatories to small instruments in almost every primary science discipline.

Many of his early designs were later developed into successful flight missions.

**Roser Juanola Parramon** received her BS and MS degrees in electrical engineering and computer science and MS degree in photonics from Polytechnic University of Catalonia, Spain, in 2008 and a PhD in astrophysics in 2014 from University College London, United Kingdom. She is currently a research engineer at NASA Goddard Space Flight Center. Her current research activities include modeling coronagraph instruments and corresponding wavefront sensing and control.

**Avi M. Mandell** is a scientist in the Planetary Systems Laboratory at NASA Goddard. He works on analyzing observations of transiting and directly imaged exoplanets and circumstellar disks, as well as modeling spectra of planetary atmospheres and the dynamical evolution of planetesimals during the formation of terrestrial planets. He is the director of the GSFC Sellers Exoplanet Environments Collaboration and is the instrument project scientist for the coronagraph integral field spectrograph for the WFIRST space telescope.

**Garrett J. West** received his BS and MS degrees in optics from the Institute of Optics at the University of Rochester. He is an optical engineer and optical designer at NASA's Goddard Space Flight Center. He designs and analyzes the next generation of NASA's optical instruments and space telescopes. His optical engineering experience spans from small internal research efforts to large international missions, such as the James Webb Space Telescope (JWST). His research focus is in freeform optics, where he investigates designs with reduced volume, fewer mirrors, wider fields of view, and better image quality to meet the growing needs of NASA science missions.

**Neil T. Zimmerman** is a research astrophysicist in the Exoplanets and Stellar Astrophysics Laboratory at NASA's Goddard Space Flight Center. He is a member of the WFIRST Project Science team contributing to the development of the coronagraph instrument. He completed his PhD in astronomy at Columbia University in 2011. Before starting his position at Goddard in 2017, he worked at the Max Planck Institute for Astronomy, Princeton University, and the Space Telescope Science Institute.